Journal of Zhejiang University-SCIENCE A (Applied Physics & Engineering)
ISSN 1673-565X (Print); ISSN 1862-1775 (Online)
www.jzus.zju.edu.cn; www.springerlink.com
E-mail: jzus@zju.edu.cn

Modelling and validation of a roller-cam rail mechanism used in a 2D piston pump*

Ding-can JIN[†1], Jian RUAN[†‡1], Sheng LI[1], Bin MENG[1], Ling-feng WANG[2]

[1]*Key Laboratory of E&M, Zhejiang University of Technology, Hangzhou 310023, China*

[2]*Beijing Aerospace Technology Institute, Beijing 100000, China*

[†]E-mail: jindingcan@163.com; ruanjiane@zjut.edu.cn

Received Feb. 2, 2018; Revision accepted Sept. 14, 2018; Crosschecked Jan. 7, 2019

Abstract: The 2D principle is a new concept in hydrostatic pump design. It features a piston with a compound motion of both rotation and reciprocation to realize the functions of pumping and distribution. The compound motion is achieved through a specially designed roller-cam rail mechanism. Compared with conventional axial piston pumps, the 2D pump avoids sliding friction pairs completely and optimizes the force balanced conditions in the pump, making it easier to operate at the condition of higher speeds. The pump is also highly integrated for four cycles of suction and delivery for each round of the piston and thus has increased power density. Additionally, by applying a pair of pump units in tandem, the pump eliminates the structural flow ripple, caused by the limited number of pump elements, which exists in traditional pumps. The performance of the proposed 2D pump is highly dependent upon the motion conversion mechanism, especially the roller-cam rail mechanism. A mathematical model of the cam rail is developed and compared with its experimental counterpart to demonstrate its precision. Then, the performance of the piston and the no-load flow characteristics of the tandem pump are tested and analyzed to show the effectiveness of the roller-cam rail mechanism and the viability of the tandem pump. Although the curves of no-load flow characteristic of the tandem pump include a lot of clutter, by analyzing the frequency spectrogram of the curves of flow and revolving speed, they can be smoothed by applying a band-pass filter to remove that clutter. For comparison, the flow ripple in the experimental and simulation results of the tandem pump is smaller than that in simulation results of the traditional piston pump at low pressure. Both the theoretical analysis and experimental results indicate that the surface of the cam rail is precise and the pump has the potential advantage of eliminating sliding friction pairs and flow ripple.

Key words: Two-dimensional piston pump; Functions integration; Roller-cam rail mechanisms; Mathematical model; Zero structural flow ripple

https://doi.org/10.1631/jzus.A1800085 **CLC number:** TH321

1 Introduction

High power density is one of the greatest advantages of fluid power technology and makes it widely employed in industry, especially for drives and actuators in mobile applications. Among these applications, axial piston pumps are the most common in hydraulic systems where heavy power and high pressure are required (Ivantysynova, 2008). In the axial piston pump there are some irreplaceable sliding friction pairs, which generate hydraulic supports for the reciprocating motion of the piston and the rotation of the cylinder, and thus realize the oil suction and delivery of the pump. Since the introduction of the axial piston pump in hydraulic systems, researchers have been focusing their attention on its sliding friction pairs to improve it.

The swash-plate type pump including the piston/cylinder pair, the slipper/swash-plate pair, and the

‡ Corresponding author

* Project supported by the National Natural Science Foundation of China (No. 51675482)

ORCID: Ding-can JIN, https://orcid.org/0000-0002-3896-277X; Jian RUAN, https://orcid.org/0000-0002-3476-2359

cylinder/valve-plate pair, and the bent-axis type pump replace the slipper/swash-plate pair with a spherical-joint/disk pair (Manring and Zhang, 2000; Hong and Doh, 2004). Ideally, the clearance between these sliding friction pairs is full of lubricating oil because of the hydrostatic and hydrodynamic bearing effect. However, due to the restriction of force balances resulting from mechanical design and tribology problems in the relative sliding parts, the maximum pressure and speed between the sliding parts are significantly limited. Additionally, the lubricating oil itself will cause power loss. That means there is a virtual limitation on the power density of the axial piston pump (Manring et al., 2014).

In addition, the noise of axial piston pumps is relatively high compared with the noise of electrical motors and thus makes the pump less competitive in many applications (Turner et al., 2006). Fluid-borne noise is considered to be the biggest source of noise in hydraulic systems and flow fluctuations are the main contribution to that (Mehta, 2006). It is also known that flow variation is basically caused by the finite number of pistons and by the compressibility of the fluid.

Among the friction pairs of the axial piston pump, the cylinder/valve-plate pair plays a very important role. It not only determines the power density of the pump, but also, to a large extent, influences its flow ripple as has been highlighted in (Ma et al., 2010; Cho, 2015). Therefore, improvements in power density and hydraulic noise level remain huge challenges for the development of hydraulic axial piston pumps, and specifically for the cylinder/valve-plate pair (Manring et al., 2013; Xu et al., 2016; Zhang et al., 2018).

To minimise the limitation of the friction pairs on power density and reduce the flow ripple in the axial piston pump, a better design of the component geometry of friction pairs is effective, and innovative structures may also offer feasible choices. Vael et al. (2003) proposed a 'floating cup principle' where two pumps are connected by a through shaft to make a tandem pump. It was shown that the flow and pressure pulsations were greatly reduced resulting in low noise due to the very large number of pistons. Navarro (2011) proposed a volumetric pump in which the flow is distributed by the piston. The compound movement of the piston transmitted by the rotor involves bi-directional linear and angular movements. Through that, the piston delivers a steady flow rate. However, the rotor brings an additional sliding friction pair and the speed may be limited by the swinging motion of the piston (Navarro, 2011). Luo et al. (2011) worked on an axial piston water-pump utilizing the principle of the piston valve. This structure initially appeared in the hydraulic motors produced by the Parker Hannifin Company, USA, which distributed the flow through the collaboration of four pistons. By means of the piston valves, they eliminated the structure of cylinder/valve-plate pair and thus reduced the abrasion phenomenon and pressure ripple in axial piston water-pumps. Du et al. (2016) introduced a rotary valve to replace the check valve in a single-piston axial piston pump. With the rotary valve, the pump could achieve high speed flow distribution. In addition, in order to reduce torque ripple and thus the noise of the piston pump, Manring et al. (2007) integrated the flow of two conventional axial piston pumps as a tandem pump so as to increase the number of pistons. They also analyzed the factors affecting torque ripple and noise, such as the index angle of the swash plate and the parity of the numbers of pistons. It becomes clear that, firstly, increasing the number of pistons can reduce the flow and pressure pulsations but it will not eliminate them; secondly, integrating the function of flow distribution into the piston, the abrasion phenomenon and pressure ripple can be reduced; thirdly, rotation of the piston leads to faster flow distribution.

In recent decades, here, in the Zhejiang University of Technology, intensive research has been conducted on the development of novel hydraulic control valves using both rotary and linear motions of a single spool, namely 2D valves (Ruan et al., 2001, 2002). In particular, the 2D vibration exciting valve (Ruan and Burton, 2009), which alternately directs oil flow through valve ports to excite the vibration of a hydraulic actuator, left a clue for the further development of flow distribution in the novel hydraulic pump proposed in this paper. The new principle, the '2D piston pump', has the potential to combine the advantages of current axial piston pumps and the novel principles mentioned above:

1. The number of main friction pairs is decreased to two by integrating the flow distribution function

with the rotation of the piston, while the function of oil delivery is realized by the linear motion of the piston at the same time.

2. Leakage is reduced by reduction of friction pairs and the replacement of the slipper/swash-plate pair or the spherical-joint/disk pair by a rolling friction pair.

3. All the forces in the pump are balanced by the symmetrical structure, so eccentric motion of the piston due to unbalanced forces will not appear.

4. The ceiling limitations of pressure and velocity are enhanced and the contradiction between lubrication and leakage of the friction pairs is avoided.

5. It is highly integrated with four cycles of suction and delivery per round of the piston to increase its working efficiency.

6. The flow variation caused by the finite number of pistons in the traditional pump is eliminated by the tandem structure with two pistons.

However, there are also some concerns. The new principle is highly dependent on the motion transfer mechanism because the advantages detailed above are premised upon an excellent motion transfer device, namely the roller-cam rail mechanism. As the motion transfer device connects the rotation of the motor shaft and the compound motion of the piston, it needs to be improved in respect of fatigue strength, speed limit, and precision. That will also ensure the improvement of pressure and velocity and the elimination of the structural flow ripple in the unit pump. Thus, the mathematical model and contact law of roller-cam rail mechanism were constructed and analyzed. This study will focus on the characteristic of the roller-cam rail mechanism and the 2D tandem piston pump, and will verify the feasibility of the new principle.

2 Two-dimensional piston pump

A brief review of the conventional axial piston pump will help understanding of the proposed 2D piston pump. As shown in Fig. 1b, there are four main sliding friction pairs or sliding bearings in a swash-plate axial piston pump: the slipper/swash-plate pair, the piston/cylinder pair, the cylinder/port plate pair, and the ball joint/slipper pair. On account of the higher requirement of pressure and flow rate in the conventional axial piston pump, the friction pairs play crucial roles under heavy load and high-speed working conditions. Lubrication is realized by introducing high pressure oil into the gaps of the friction pairs. Ideally, the clearances of these gaps are homogeneous and full of lubrication oil. The oil not only provides a continuous and stable support for the piston load, but also plays the key role of lubrication and removal of heat from friction pairs when the pump is working at high speed and heavy load. However, this process is accompanied by leakage because of the lubrication. Here arises a contradiction: adequate lubrication will increase the leakage and decrease the efficiency of the pump; to increase the volumetric efficiency of the pump, the leakage has to be kept low. In that condition, the heat of oil in friction pairs will increase and the working condition of friction pairs will deteriorate or even cause abrasion of the friction pairs. Moreover, as shown in Figs. 1a and 1b, the elements of the friction pairs cannot practically remain parallel, because there are unbalanced forces. Those forces are caused by the inclined swash-plate, the asymmetric distribution slots on the valve plate, and the centrifugal forces produced by the rotation of the cylinder. Thus, direct metal contacts will certainly occur and limit the relative velocity, which in

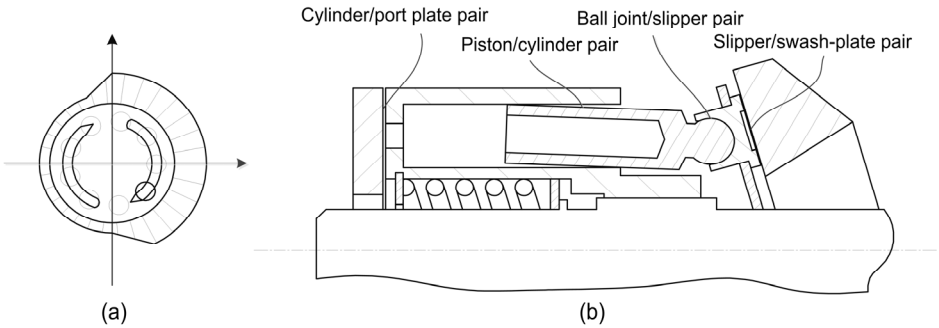

Fig. 1 Main friction pairs and force balanced condition of a swash-plate axial piston pump
(a) Pressure distribution in cylinder/port plate pair; (b) Main friction pairs

turn causes deterioration of the force balanced conditions of the pump elements. The deteriorated conditions of pistons, cylinder, and slippers will create even tougher contradiction between lubrication and leakage.

In order to get rid of sliding friction pairs and improve force balanced conditions in the conventional piston pump, a 2D piston pump is proposed in this study. The piston of the pump is driven by two spatial cam-follower mechanisms installed at two ends of the cylinder. As shown in Fig. 2, there are two closed working chambers formed inside the cylinder between the end surfaces of the piston and the special cams respectively. By the fork-roller coupler and spatial cam-follower mechanism, the rotation coming from the motor or engine (power coming from motor or engine) is transformed into the compound movement of the piston, involving rotation and linear reciprocation. As a result, the volumes of the two working chambers are alternately changed. The pump sucks the oil from the low-pressure windows and delivers the oil to the high-pressure windows through the distributing grooves around the piston.

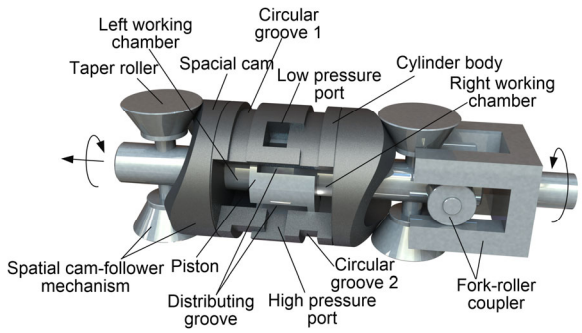

Fig. 2 Partial sectional view of a 2D piston pump

The detailed functioning processes of the pump are illustrated in Figs. 3a–3d. There are four windows distributed uniformly around the cylinder which are labeled *A*, *B*, *C*, and *D* in sequence. Under the premise that the fork-roller coupler rotates as shown in Figs. 3a–3d, the windows *A* and *C* are connected to the circular groove 1 linked with the outlet or high-pressure port of the pump, whereas the windows *B* and *D* are connected to the circular groove 2 linked with the inlet or low-pressure port of the pump. Correspondingly, there are four grooves distributed uniformly around the piston which are labeled *E*, *F*, *G*, and *H* in sequence. The grooves *E* and *G* are linked with the right chamber and the grooves *F* and *H* are linked with the left chamber. The roller-cam mechanism is composed of a spatial cam mounted at the two ends of the cylinder and a tapper roller fixed to the piston rods through crossed pin axes. When the piston is driven by the motor or engine with the fork-roller coupler and rotates in the direction shown in Figs. 3a–3d, it also makes a reciprocating motion due to the constraint from the roller-cam rail mechanisms. As the motion phase of the piston changes gradually from Fig. 3a to Fig. 3b, the volume of the left chamber decreases and the oil in red inside is pumped out through the distributing grooves *H* and *F* to the high pressure windows *A* and *C*, and is then gathered in the circular groove 1.

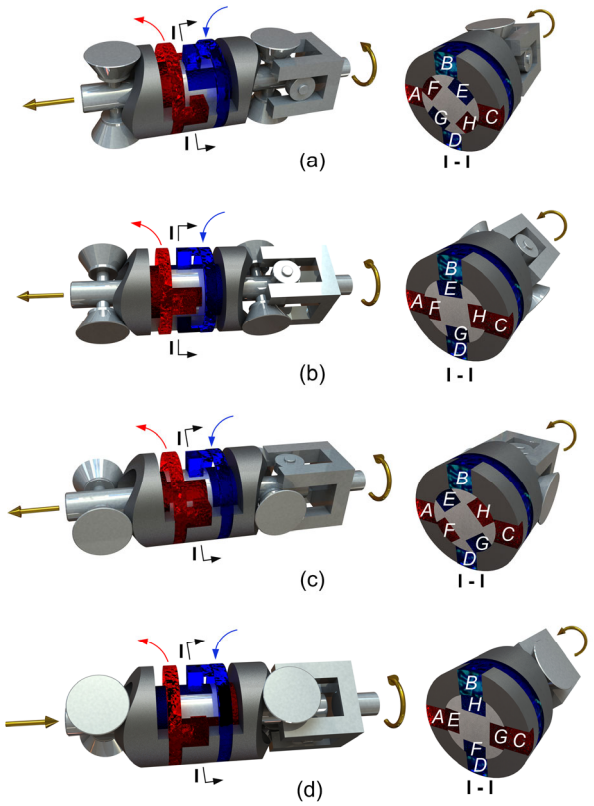

Fig. 3 Detailed functioning processes of the pump
(a) Rotation angle at 0°; (b) Rotation angle at 45°; (c) Rotation angle at 90°; (d) Rotation angle at 135°

In the meantime, the volume of the right chamber is increasing and the oil in blue is sucked in through the low-pressure windows *B* and *D* (which

are linked with the circular groove 2) to the distributing grooves *E* and *G*. In the progress from Fig. 3a to Fig. 3b, the overlapping areas between the windows and distributing grooves are increasing until arriving at a peak. At the same time, in the process of moving from Fig. 3b to Fig. 3c, the overlapping areas between the windows and distributing grooves decrease until fully closed. Compared with Fig. 3a, the piston in Fig. 3c has rotated 90° and has reached the far left of its working position. In the meantime, the left chamber finishes its function of pumping and the right one finishes its function of sucking. As the piston keeps on rotating, it will reverse its linear motion. When the piston reverses its linear motion, the two chambers in the pump exchange their functions and play a diametrically opposite role as shown between Fig. 3c and Fig. 3d, as the angle of the piston changes from 90° to 135°. In the piston rotating angle from 90° to 180°, the volume of the right chamber decreases and the oil inside is pumped out through the distributing grooves *G* and *E* to the high-pressure windows *A* and *C*. Meanwhile, the volume of the left chamber increases and the oil is sucked in through the distributing grooves *H* and *F* from the low-pressure windows *B* and *D*. As the piston continues to rotate, the process above from Fig. 3a to Fig. 3c is repeated for every 180°, i.e. the cycle of the pump is 180°. More specifically, the functions of the four windows *A*, *B*, *C*, and *D* and the two circular grooves 1 and 2 are constant, but the working conditions of the grooves *E*, *G*, *H*, *F* and the two working chambers are shifting, and every working chamber sucks and delivers twice in a rotation of 360°, which means the 2D piston pump with two working chambers sucks and delivers four times per round of the piston.

When the pump is working, its displacement *q* is proportional to the area *A* of the chamber and the stroke *h* of the cam, and can be expressed as

$$q = 4Ah. \tag{1}$$

From the analysis above, it can be clearly seen that the 2D piston pump gets rid of the sliding friction pairs that are main factors affecting the promotion of pressure and velocity in the conventional piston pump. The slipper/swash-plate pair is replaced by the rolling friction pair, and the cylinder/port plate friction pair is eliminated by integrating the function of flow distribution into the rotational piston. Thus, the ceiling limitations of pressure and velocity are enhanced and the contradiction between lubrication and leakage of the friction pairs is avoided. Besides, the force balanced conditions are also greatly improved. The 2D piston pump gets rid of all the tilting moments by applying the symmetrical roller-cam rail mechanism, when the tilting moments constantly act on key elements of the conventional axial piston pump. The tilting moments can be divided into the tilting moment of the piston produced by the counteraction of the swash-plate, the tilting moment of the slipper produced by centrifugal force, and the tilting moment of the rotors caused by the inertia of the reciprocating pistons. Finally, by comparison with the conventional axial piston pump, the structure of the 2D piston pump is greatly simplified and the power density is significantly enhanced.

However, there is still a problem with the 2D piston pump: the flow ripple coming from the structure. Two chambers of the pump vary with the phase angle of 180°, so that when one chamber is sucking, the other will be pumping, and vice versa. Since the piston is making a reciprocating motion, a variation in the speed becomes inevitable and thus a ripple in the flow rate of the pump is unavoidable. When the motor rotates at a constant speed, the reciprocation of the piston is decided by the shape of the cam. For example, when the motion rule of the cam is chosen as uniform acceleration and deceleration in the stroke *h*, where complete period is expressed as *T*, the displacement of the piston $f(\theta)$ and velocity of the piston $f'(\theta)$ are expressed in Eq. (2) and Eq. (3), respectively, by the angle θ that the piston rotated and the corresponding angle θ_0 when the piston rotated 1/2 of period *T*.

$$f(\theta)=\begin{cases}\dfrac{2h\theta^2}{\theta_0^2}, & \theta\in\left(0,\dfrac{T}{4}\right),\\[2ex] h-\dfrac{2h(\theta_0-\theta)^2}{\theta_0^2}, & \theta\in\left(\dfrac{T}{4},\dfrac{T}{2}\right),\\[2ex] h-\dfrac{2h(\theta-\theta_0)^2}{\theta_0^2}, & \theta\in\left(\dfrac{T}{2},\dfrac{3T}{4}\right),\\[2ex] \dfrac{2h(2\theta_0-\theta)^2}{\theta_0^2}, & \theta\in\left(\dfrac{3T}{4},T\right),\end{cases} \tag{2}$$

$$f'(\theta)=\begin{cases}\dfrac{4h\theta}{\theta_0^2}, & \theta\in\left(0,\dfrac{T}{4}\right),\\ \dfrac{4h(\theta_0-\theta)}{\theta_0^2}, & \theta\in\left(\dfrac{T}{4},\dfrac{T}{2}\right),\\ \dfrac{-4h(\theta-\theta_0)}{\theta_0^2}, & \theta\in\left(\dfrac{T}{2},\dfrac{3T}{4}\right),\\ \dfrac{-4h(2\theta_0-\theta)}{\theta_0^2}, & \theta\in\left(\dfrac{3T}{4},T\right).\end{cases} \quad (3)$$

The waveforms are also shown in the curves in Fig. 4, from which it can be clearly seen that the flow rate has a large fluctuation for the single unit of a 2D piston pump. To eliminate the structural flow ripple, two 2D piston pumps are applied in tandem, as shown in Fig. 5. The two pumps are set with a phase difference of 90° (corresponding to a rotary angle difference of 45°). Through the transmission mechanism of the fork-roller coupler, two pumps can be connected together in tandem and driven by one motor.

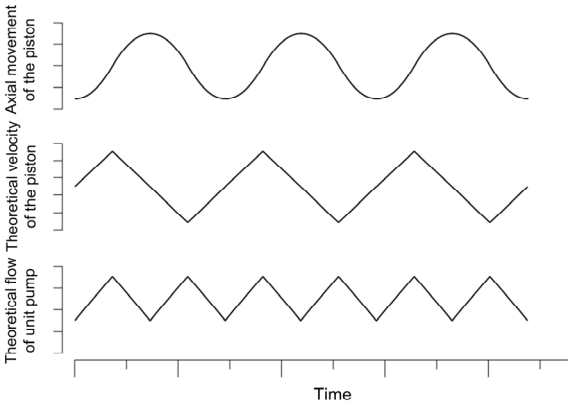

Fig. 4 Curves of the 2D piston pump

As shown in Fig. 5, two pumps were combined and thus there are two chambers in red working for the high-pressure port and two in blue for the low-pressure port. By this means the flow of the two pumps is combined. Because of the phase angle difference of 90°, when the flow of port 1 reaches its maximum value, the flow of port 2 is exactly at its minimum, and by means of the superposition of the flow from these two ports, the flow ripple is greatly reduced.

As shown in Figs. 6a and 6b, the blue curves stand for the motion and flow of pump 1, and the pink

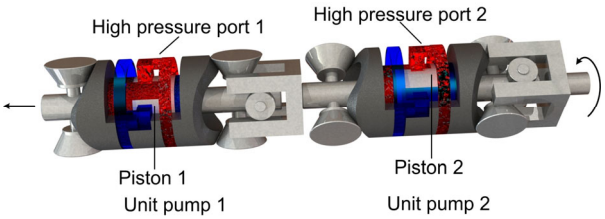

Fig. 5 Two 2D piston pumps in tandem

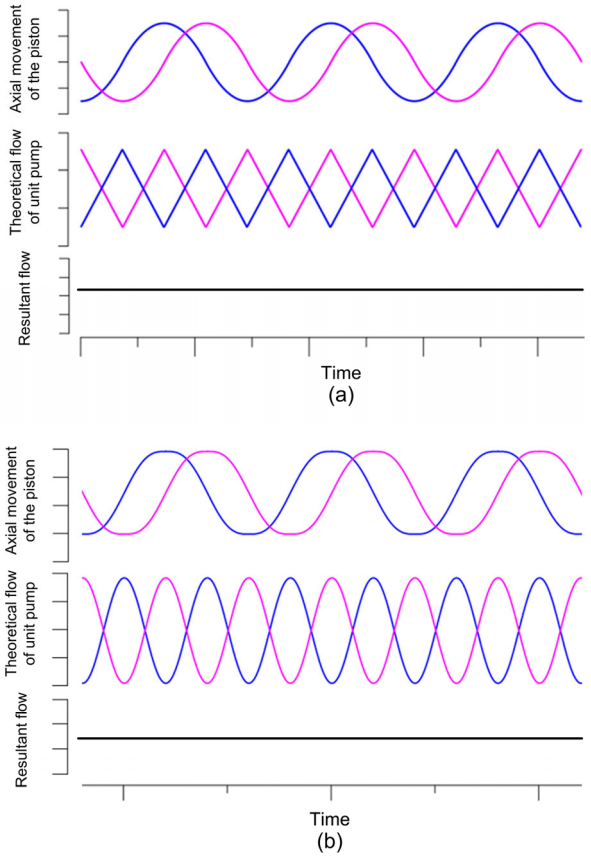

Fig. 6 Resultant flow of the tandem pump using different curved surfaces

(a) Curved surface in the law of uniform acceleration and deceleration; (b) Curved surface in the law of sinusoidal acceleration

curves stand for the motion and flow of pump 2. For the pumps in Figs. 6a and 6b, the phase angle is 90° which is decided by the structure of the 2D pump. By adopting different curved surfaces by which the consequent flow from the two pumps can be symmetrical, the curve of resultant flow is always a straight line after the superposition of the curves from two pumps in tandem, which is why the law of cosine acceleration motion is abandoned. That means the

tandem pump has the potential of lowering the noise caused by flow ripple. The advantages of the 2D pumps in tandem are highly dependent on the design of the motion transfer device, namely the roller-cam rail mechanism, which bears the heavy hydrostatic force coming from the piston in the rotary-to-linear motion transformation at high speed. Thus, a mathematical model of the contacting surface is necessary for assuring the accuracy of the motion transfer device. The curvature of the cam surface is decided by the acceleration of motion rule, and it is smaller for the law of uniform acceleration and deceleration than for the law of sinusoidal acceleration. Thus, the law of uniform acceleration and deceleration is chosen for the cam surface used in the prototype.

3 Mathematical model of the contact surface

For the roller-cam rail mechanism, the spherical roller-cam rail mechanism shown in Fig. 7 may be chosen as the motion transfer device in consideration of its convenience of design and manufacture. However, the contact area between the spherical rollers and the cam rail is small (it would be a point in the rigid condition), and the Hertz contacting stress tends to be very high. After 50 h of running-in testing at a pressure of 4 MPa and velocity of 2000 r/min, severe abrasion and wearing were clearly shown in Fig. 7. Another choice of motion transfer mechanism is the taper roller-cam rail mechanism shown in Fig. 8.

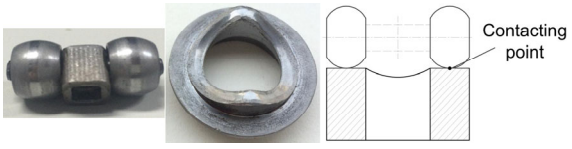

Fig. 7 Abrasion in the spherical roller-cam rail mechanism

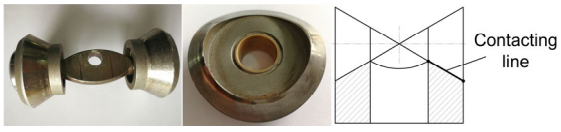

Fig. 8 Abrasion in the tapper roller-cam rail mechanism

Compared with the spherical roller-cam rail mechanism, the contacting area in the taper roller-cam rail mechanism is greater (it would be a line in the rigid condition), and the Hertz contacting stress is greatly relieved, which will certainly improve the contacting and lubrication condition abrasion between the roller and cam rail. After 50 h of running-in testing at a pressure of 6.5 MPa and velocity of 6000 r/min, the condition of this mechanism is still much better than that of the spherical roller-cam rail mechanism as Fig. 8 shows.

Because two components contact in a line in Fig. 9, the velocity distribution of points has to be considered in the case of the speed difference of the contacting points in that line. To analyze the velocity distribution, three contact points (A, B, and C) on the contact line have been chosen. The rotations of points A, B, and C are defined as V_1, V_2, and V_3 when they are rotating around the axis O-O_3, and the revolutions of points A, B, and C are defined as V'_1, V'_2, and V'_3 when they are rotating around the Z-axis. Because the extension lines of the contacting part between two taper rollers and the rail cam intersect on point O, there is a proportional variation between the turning radius of rotation and the revolution of any contacting point. That means all the contact points can get the same tangent velocity of revolution and rotation because the velocity of the contacting points is proportional to the turning radius.

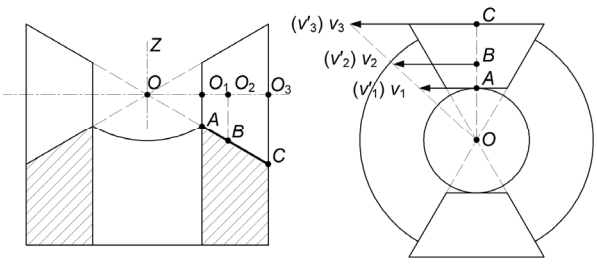

Fig. 9 Velocity distribution of points on the contacting line

After the comparison above, the taper roller-cam rail mechanism is adopted as the transfer device because of its high-speed and heavy-load features. After consideration of the force balance and velocity distribution, the bulges of the cam are set as two. As shown in Figs. 10a–10c, when the taper rollers are rotating around the Z-axis, the rollers will rotate around its central axis (namely the axis of the taper roller) in the same time, and always in contact with

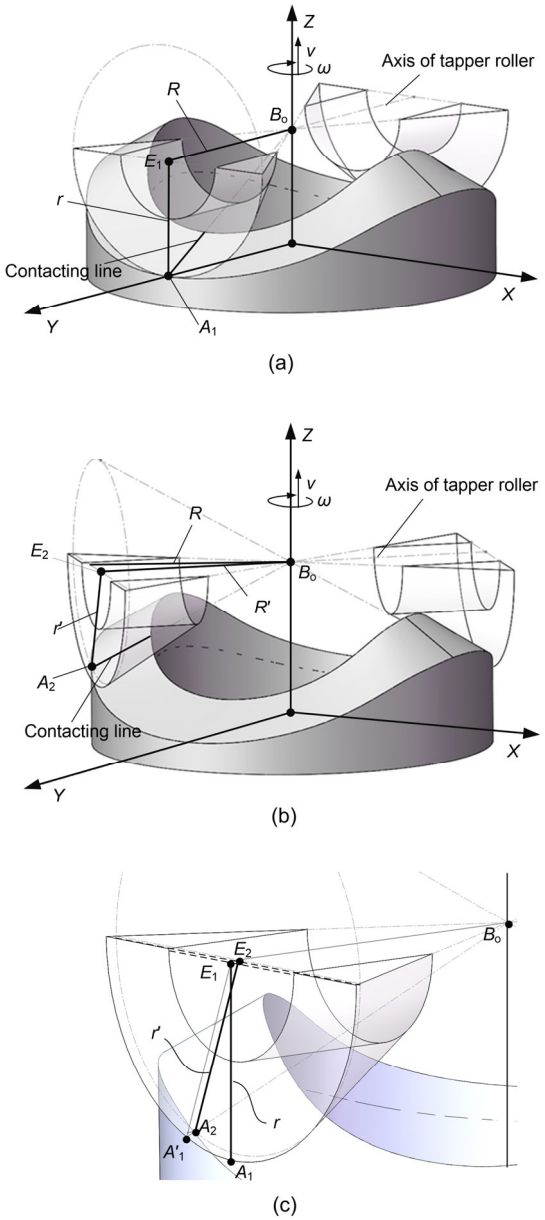

Fig. 10 Related parameters of point *A*
(a) Contacting point A_1 at 0°; (b) Contacting point A_2 at 45°; (c) Contrast of points A_1 and A_2

the surface of the cam in a contacting line. The point A is the contacting point between the most peripheral curve of the cam rail and the outer surface of the taper roller. In the process of rotation, the shortest distance between point A and the Z-axis is defined as the radius of revolution (R) and is represented as E_1B_o, and the shortest distance between point A and the axis of the taper roller is defined as the radius of rotation (r) and is represented as E_1A_1. When the point A is moving from Fig. 10a to Fig. 10b, the value of R is constant but the value of r changes because the A contact point may not be on the outer edge of the roller if the cam is inclined. By gathering the line E_1A_1 and E_2A_2 in Fig. 10c, the relationship between them is clear. It can be seen that the length of E_1A_1 is fully equal to the length of $E_1A'_1$ because they are both the radius of the outer edge of the roller. There is thus a sort of proportionality between E_1A_1 and E_2A_2 because $\triangle B_oE_1A'_1$ and $\triangle B_oE_2A_2$ are similar triangles. Depending on the relationships above, the conventional modelling approaches for a plane cam are unsuitable here, and the law of contacting point has to be used to build up a general mathematical model.

As shown in Figs. 11a–11c, the intersection of the U-axis and the Z-axis is defined as point B_o. Because point B_o is the reciprocal in the law of uniform acceleration and deceleration as the value of θ changes, the coordinate of point B_o on the Z-axis can be expressed as $(0, 0, f(\theta)+r)$. Because any point on the U-axis follows the same law, including uniform rotation around the Z-axis and reciprocation in the law of uniform acceleration and deceleration along the Z-axis, the mathematical model of point B_o is universal and the rule of its motion can be extended to all the points on the U-axis and described as B'_n. Thus, the coordinate of any point B'_n in the coordinate system can be expressed as $(\theta, R'_n, f(\theta)+r)$, when the length of B'_nB_o is defined as R'_n. Similarly, the mathematical model of the contact point A is universal, and the rule of its motion can be extended to all the points on the contacting line and be described as A_n. As the projection of point A on the central cross-section of the taper roller is defined as point B, any point A_n could be projected to the central cross-section and defined as B_n. Thus, when the coordinate of point B_n is expressed as $(\theta+\beta, R_n, f(\theta)+r)$, the coordinate of point A_n can be expressed as $(\theta+\beta, R_n, f(\theta)+r-r_n\cos\alpha)$.

According to Figs. 11a–11c, β stands for the angel of $\angle B_nB_oB'_n$, R_n stands for the length of B_nB_o, r_n stands for the length of $A_nB'_n$, and α stands for the angel of $\angle B'_nA_nB_n$.

Once the coordinate of point A_n is expressed as $(\theta+\beta, R_n, f(\theta)+r-r_n\cos\alpha)$, θ and R_n are the independent variables, and β, r_n, and α are the dependent variables. When the relationship between these three dependent

variables and the two independent variables is explicit, the coordinate of point A_n is specific. As shown in Fig. 12, $\triangle B_oB_nB'_n$, $\triangle A_nB_nB'_n$, and $\triangle B_oB'_nA_n$ share a line with each other, and the taper angle γ is a constant when the shape of the taper roller is decided. Thus, through the connection between variables α and β, the relationship between them can be expressed as Eq. (4), and the variable α can be expressed as Eq. (5).

$$\frac{\tan\beta}{\sin\alpha}=\frac{B'_nA_n}{B_nB_o}=\tan\gamma, \tag{4}$$

$$\alpha=\arcsin\left(\frac{\tan\beta}{\tan\gamma}\right). \tag{5}$$

In Fig. 12, γ stands for the angel of $\angle A_nB_oB'_n$.

When the taper roller is moving, r_n is a dependent variable related to R_n, and the relationship can be expressed as

$$r_n=R_n\cos\beta\tan\gamma. \tag{6}$$

Thus, as Eqs. (4) and (6) show, the dependent variables of point A_n can be simplified as one, namely, the dependent variable β.

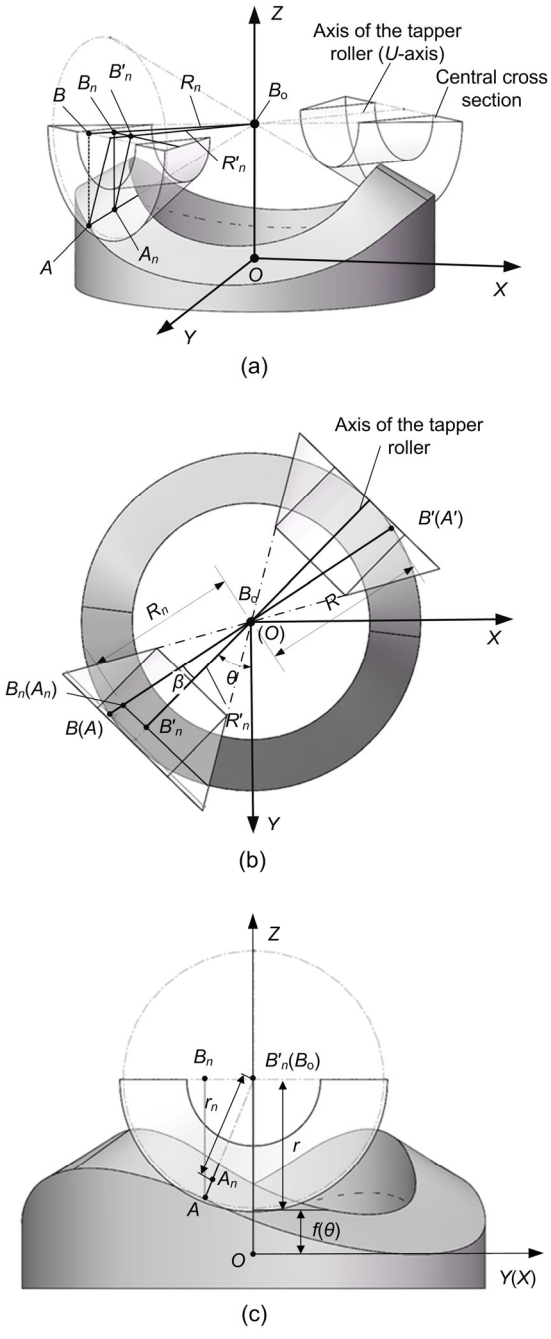

Fig. 11 Definition of points B_o, B'_n, and B_n
(a) Axonometric drawing; (b) Top view; (c) Front view

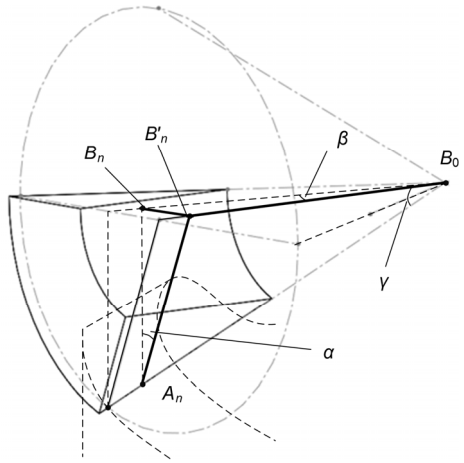

Fig. 12 Connection between variables β and α

To solve the dependent variable β, an auxiliary cycle, tangent to the corresponding curve of the cam rail, and an auxiliary angle α' are put forward as shown in Figs. 13a and 13b. Because the auxiliary cycle is vertical to the line B_oB_n, and generates an intersection point C_n with the extended line of $B_oB'_n$, the line C_nB_n is vertical to the line B_oB_n. Because $\triangle B_oB_nB'_n$ is vertical to the Z-axis, the velocity of point C_n on the surface of the auxiliary cycle is the same as that of point B_n. As the rotation radius of B_n around Z-axis is R_n, the velocity of point C_n (namely the slope

k) can be expressed as shown in Eq. (7): the trajectory of point C_n is equivalent to the expansion of a curve with the motion rule of uniform acceleration and deceleration at the rotation radius of R_n.

$$k=f'(\theta,R_n)=\begin{cases}\dfrac{4h\theta R_n}{\left(\dfrac{\pi}{2}R_n\right)^2}, & \theta R_n\in\left(0,\dfrac{T}{4}\right),\\ \dfrac{4h\left(\dfrac{\pi}{2}R_n-\theta R_n\right)}{\left(\dfrac{\pi}{2}R_n\right)^2}, & \theta R_n\in\left(\dfrac{T}{4},\dfrac{T}{2}\right),\\ \dfrac{4h\left(\dfrac{\pi}{2}R_n-\theta R_n\right)}{\left(\dfrac{\pi}{2}R_n\right)^2}, & \theta R_n\in\left(\dfrac{T}{2},\dfrac{3T}{4}\right),\\ \dfrac{-4h\left(\pi R_n-\theta R_n\right)}{\left(\dfrac{\pi}{2}R_n\right)^2}, & \theta R_n\in\left(\dfrac{3T}{4},T\right).\end{cases} \tag{7}$$

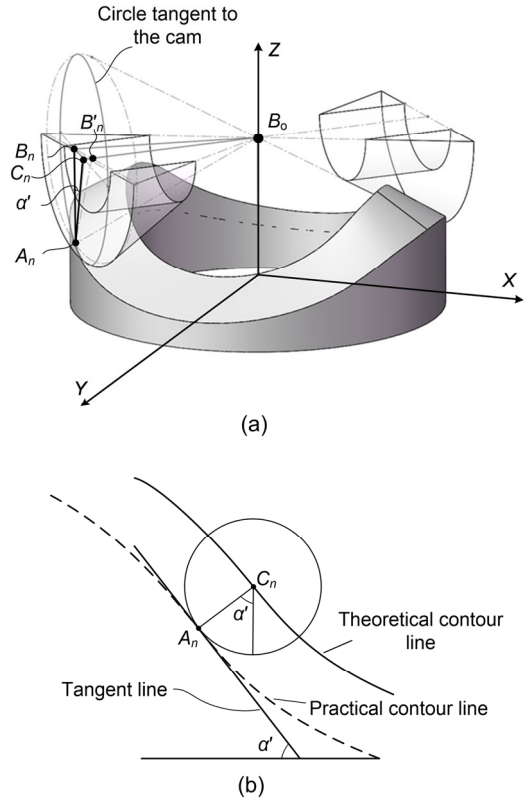

Fig. 13 Definition of α'

(a) α' in axonometric drawing; (b) α' in the cycle tangent to the cam

As Fig. 13b shows, the center of the auxiliary cycle C_n is moving along the expansion of the theoretical curve, and the auxiliary cycle is tangent to the expansion of the practical contour line at point A_n, thus the line A_nC_n is vertical to the theoretical curve and the practical curve at the same time. These two lines therefore have the same slope, k, expressed as in Eq. (7) at points A_n and C_n, and the variable α' can be expressed as

$$\alpha'=\arctan f'(\theta,R_n). \tag{8}$$

In Fig. 14, as $\angle B_nB'_nB_o$, $\angle C_nB_nB_o$, $\angle B_oB'_nA_n$, and $\angle C_nB_nA_n$ are right angles, the relationship between α' and β can be expressed as

$$C_nB_n=B_nB_o\tan\beta=R\tan\beta, \tag{9}$$

$$\begin{aligned}C_nA_n&=\sqrt{A_nB_n'^2+C_nB_n'^2}\\&=\sqrt{\left(B_0B_n'\tan\gamma\right)^2+\left(B_nB_n'\sin\beta\right)^2}\\&=\sqrt{\left(R\cos\beta\tan\gamma\right)^2+\left(R\tan\beta\sin\beta\right)^2},\end{aligned} \tag{10}$$

$$\begin{aligned}\alpha'&=\arcsin\left(\frac{C_nB_n}{C_nA_n}\right)\\&=\arcsin\left(\frac{1}{\sqrt{\sin^2\beta+\dfrac{\tan^2\gamma\cos^4\beta}{\sin^2\beta}}}\right).\end{aligned} \tag{11}$$

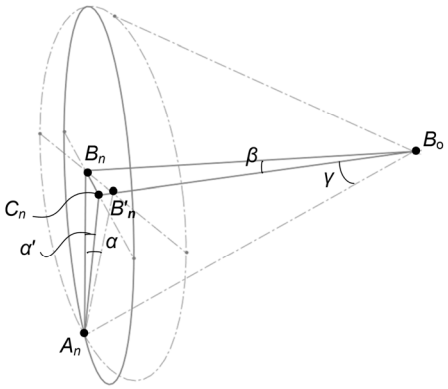

Fig. 14 Relationship between β and α'

Obviously, through the relationship between α' and θ expressed in Eq. (8) and the relationship

between α' and β expressed in Eq. (11), the dependent variable β can be expressed by θ and solved through the implicit function theorem.

Thus, any contacting point between the roller and cam can be defined as $A_n(\theta, R_n)$ and the coordinate of point A_n is expressed as $(\theta+\beta, R_n, f(\theta, R_n))$, in which the dependent variable β is defined by $f'(\theta, R_n)$ and the Z-axis coordinate of point A_n is $f(\theta, R_n)$, which can be expressed as

$$f(\theta, R_n)=\begin{cases}\dfrac{2h(\theta R_n)^2}{\left(\frac{\pi}{2}R_n\right)^2}+r', & \theta R_n\in\left(0,\ \dfrac{T}{4}\right),\\ h-\dfrac{2hR_n^2\left(\frac{\pi}{2}-\theta\right)^2}{\left(\frac{\pi}{2}R_n\right)^2}+r', & \theta R_n\in\left(\dfrac{T}{4},\ \dfrac{T}{2}\right),\\ h-\dfrac{2hR_n^2\left(\theta-\frac{\pi}{2}\right)^2}{\left(\frac{\pi}{2}R_n\right)^2}+r', & \theta R_n\in\left(\dfrac{T}{2},\ \dfrac{3T}{4}\right),\\ \dfrac{2hR_n^2(\pi-\theta)^2}{\left(\frac{\pi}{2}R_n\right)^2}+r', & \theta R_n\in\left(\dfrac{3T}{4},\ T\right),\end{cases} \tag{12}$$

$$r'=r-r_n\cos\alpha. \tag{13}$$

4 Results

After translating the mathematical model of point A_n into the Matlab programming language, the surface of the cam can be calculated and expressed by the combination of points A_n as in Fig. 15, and the accuracy of the model is decided by the value interval of θ and R_n.

As shown in Figs. 16a–16c, from the data of the coordinate of the contacting point A_n extracted from the Matlab program, the 3D model of the cam in the Solidworks program can be established and then be manufactured in the computer numerical control machine tool. After that, the entity is scanned through the instrument named 3Shape and compared with the model in the Geomagic program. Excepting those navy blue and oriental red parts caused by the chamfer and fillet on the entities, the result shows that the maximum space surface errors between the model and the entity are less than 30 μm. The maximum errors exist on the inner peak of the cam surface, and are mainly caused by heat deformation. They are shown in light blue. Then, an experiment is applied to verify the influence of the cam rail on the motion of the piston. The testing apparatus is shown in Fig. 17.

As shown in Fig. 17, the tandem pump is driven by a stepper motor which is controlled by the signal generator, and the reciprocation of the piston was tested by a laser displacement sensor to verify the conversion accuracy of the roller-cam rail mechanism. When the testing apparatus is working, the signal of the laser displacement sensor is captured and compared with the theoretical curve in the oscilloscope. The result is shown in Fig. 18.

Fig. 18 shows the contrast between the experiment result and the theoretical curve when the rotation speed of the motor is 515 r/min, in which the black line is the theoretical curve and the red one is the measured curve. There are some fluctuations on the peak and trough of the wave which were mainly caused by the surface error of the cam and the assembly error of the unit pump, but the result is basically in accord with the analysis of the surface error in Fig. 16. After the conversion accuracy of the roller-cam rail mechanism was verified, we designed a testing system to test the flow characteristic of the tandem pump and verify the influence of the roller-cam mechanism on the flow characteristics of the pump. The schematic diagram of the testing system is shown Fig. 19.

The auxiliary pump is adopted to supply oil for the 2D tandem piston pump and the relief valve is applied to simulate the load of the system. In the process of running, the speed sensor and flow meter are chosen to test the dynamic characteristics of the pump, and to verify if the pump can achieve zero structural flow ripple. The accelerator is adopted for getting wider speed range and has a torque limiter for safety considerations. The components are then installed on the platform and experiments are done to verify the performance of the pump.

The test bench is shown in Fig. 20. Through the test bench, the curve of flow and revolving speed of

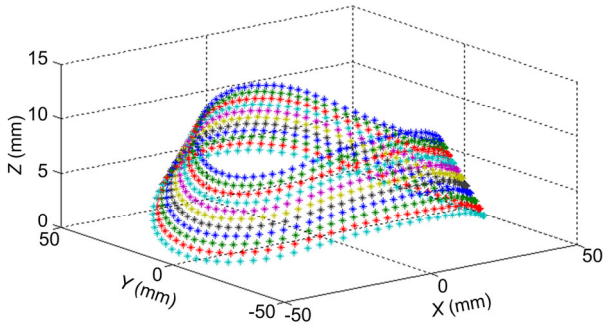

Fig. 15 Cam surface combine of points A_n

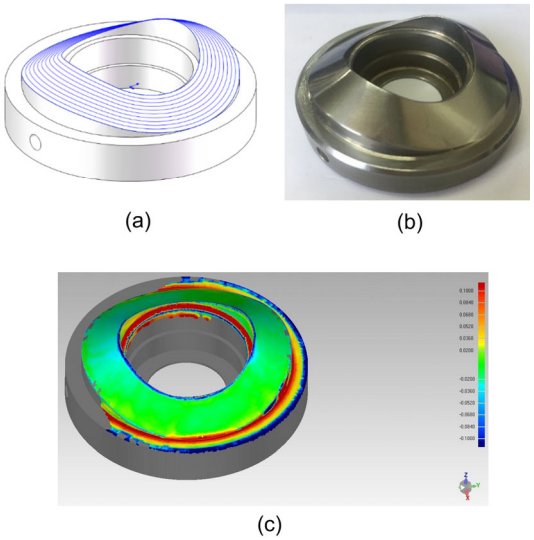

Fig. 16 Contrast (mm) between 3D model and entity shows in color

(a) 3D model; (b) Cam manufactured; (c) Contrast result in Geomagic

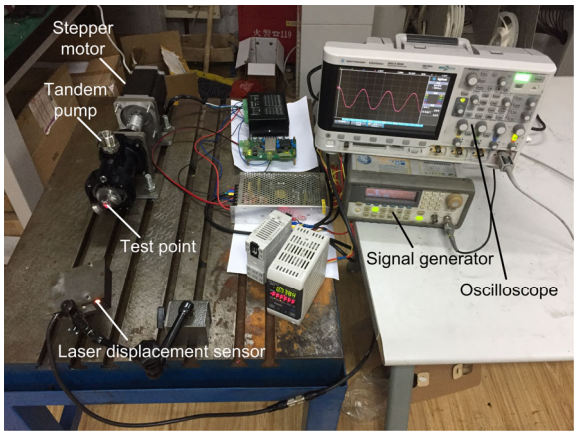

Fig. 17 Test rig of tapper roller-cam rail mechanism

the 2D tandem pump at a pressure of 0.3 MPa are tested and shown in Figs. 21 and 22.

Figs. 21a–21c show the flows corresponding to different revolving speeds in black and blue

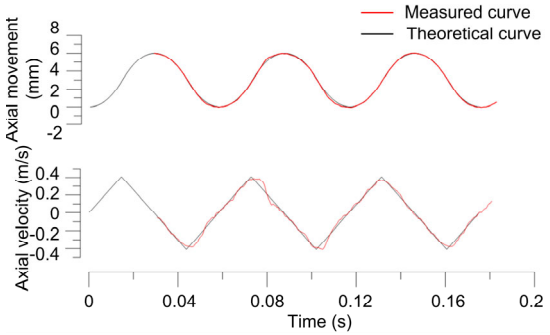

Fig. 18 Contrast between the measured and theoretical curves

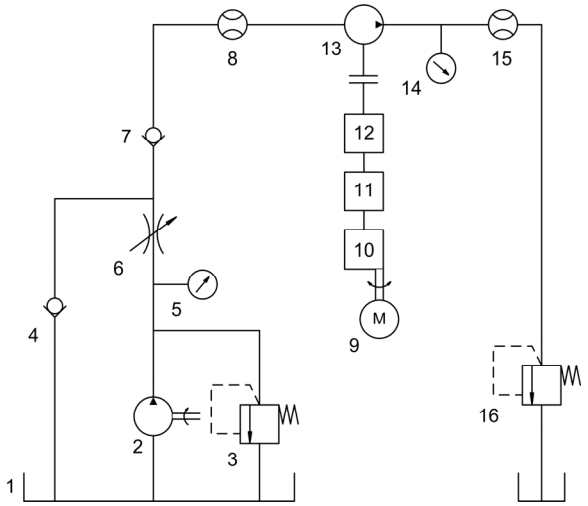

Fig. 19 Schematic diagram of the testing system

1: oil tank; 2: auxiliary pump; 3: relief valve; 4: check valve; 5: pressure gauge; 6: throttle valve; 7: check valve; 8: flow meter; 9: motor; 10: accelerator; 11: torque limiter; 12: torque and speed sensor; 13: 2D tandem piston pump; 14: pressure gauge; 15: flow meter; 16: relief valve

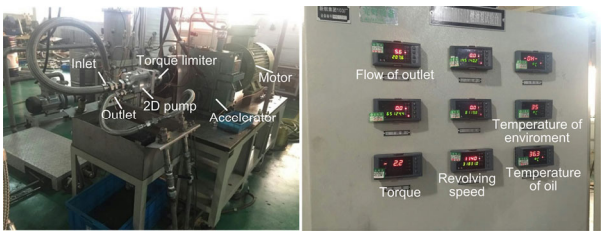

Fig. 20 Test bench of the tandem pump

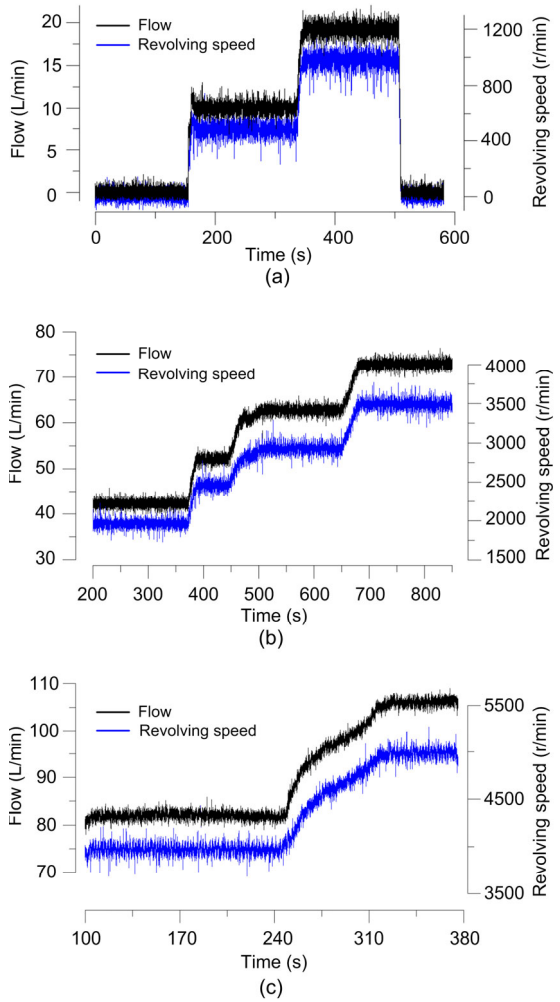

Fig. 21 Testing curves of flow and revolving speed
(a) At the lower region; (b) At the middle region; (c) At the higher region

respectively when the pump is working, and show that the flow characteristics of the 2D tandem pump are linear at different revolving speeds.

As there exist non-negligible fluctuations of flow and revolving speed in Fig. 21, the partial curves of Figs. 21a–21c are amplified in Figs. 22a–22c. After the amplification, it is obvious that the tendencies of the curves of flow and revolving speed are consistent. For instance, the experimental flow ripples of the 2D tandem pump are 14.63%, 10.11%, 7.89%, and 3.70% near the speeds of 1000 r/min, 2000 r/min, 3500 r/min, and 5000 r/min, respectively, when the corresponding speed ripples are 20.56%, 14.30%, 10.81%, and 5.83%. To obtain a quantitative description of the flow characteristics, a fast Fourier transform is performed on the points that make up the curve in Fig. 21. Through the transform, the frequency composition of two curves can be detected, which can explain the following features between the curves of flow and revolving speed, and remove clutter from the two curves.

By plotting the frequency spectrogram of the two curves near the speeds of 1000 r/min, 2000 r/min, 3500 r/min, and 5000 r/min using logarithmic coordinates, the consistency of frequency distribution in two curves is obtained and is shown in Figs. 23a–23d. Through that, the inconsistent frequency band intervals are determined as 5–47 Hz, 10–47 Hz, 15–47 Hz, and 15–47 Hz, respectively. Depending on the frequency spectrogram above, the curve composed of a series of discrete data points can be smoothed by applying a band-pass filter on the data in the Matlab program.

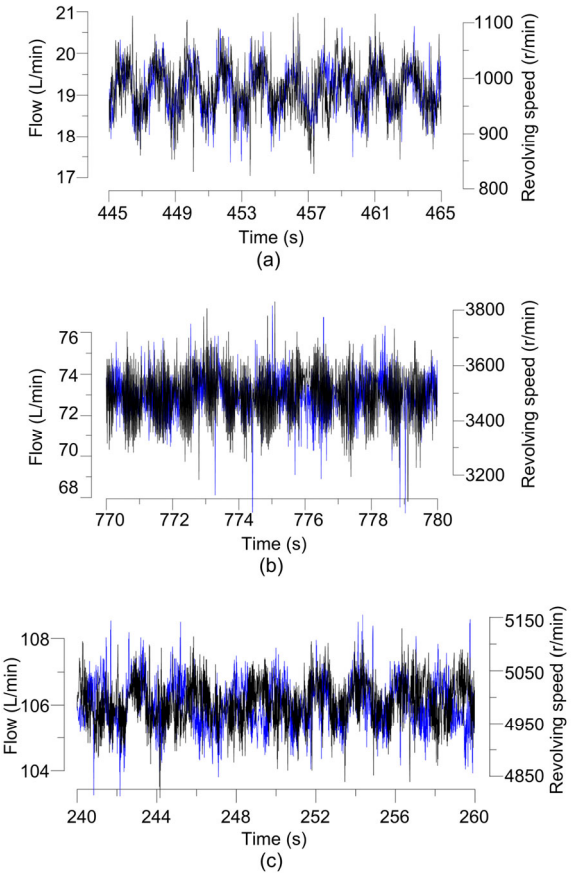

Fig. 22 Partial view of Fig. 21
(a) Partial view of Fig. 21a; (b) Partial view of Fig. 21b; (c) Partial view of Fig. 21c

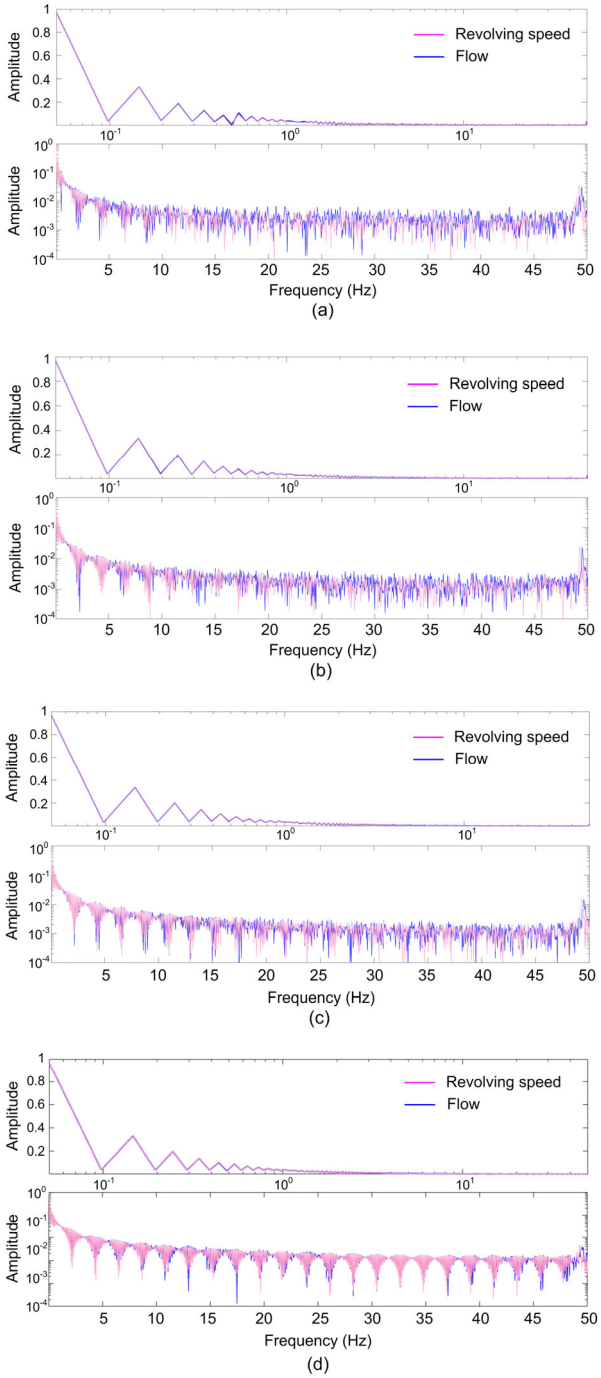

Fig. 23 Frequency spectrogram of the curves of flow and revolving speed

(a) At the revolving speed near 1000 r/min; (b) At the revolving speed near 2000 r/min; (c) At the revolving speed near 3500 r/min; (d) At the revolving speed near 5000 r/min

Partial curves of flow and revolving speed in Fig. 21 after the use of a band-pass filter are selected and shown in Figs. 24a and 24b. The clutter is removed and the curve looks close to the theoretical one. Thus, the filtered experimental flow ripples of the 2D tandem pump are 4.10%, 3.70%, 3.24%, and 0.85%, respectively, when the corresponding speed ripples are 11.42%, 7.32%, 5.55%, and 1.68%. The result shows that the structural flow ripple is eliminated after the clutter is filtered.

As the sampling frequency of the test bench is 100 Hz, it is unable to find the flow ripple caused by reverse flow and show the fluctuations in detail. Thus, through the Amesim program, the flows of a traditional pump with seven pistons and the 2D tandem pump are calculated. The flows of the two pumps at the revolving speeds of 1000 r/min, 2000 r/min, and 3500 r/min are compared in Fig. 25. The flow ripples of the traditional pump are 4.50%, 4.83%, 5.64%, and 6.60% when the flow ripples for the 2D tandem pump are calculated at 1.00%, 1.24%, 1.70%, and 2.60%, respectively.

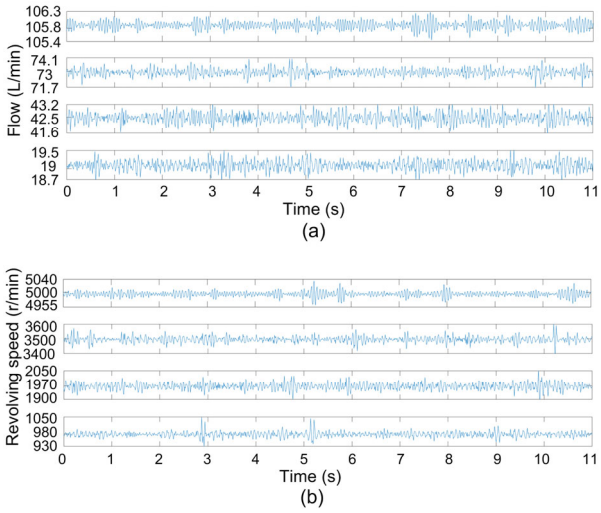

Fig. 24 Curves after the use of a band-pass filter

(a) Curve of flow; (b) Curve of revolving speed

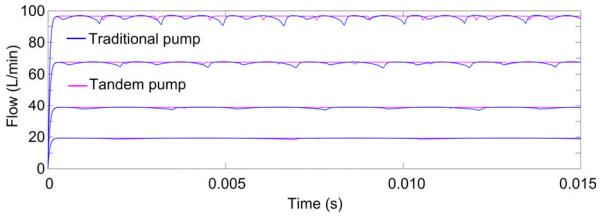

Fig. 25 Flow curves of traditional piston pump and tandem pump from the simulation

Through simulation and experiment, the flow and revolving speed ripples of the 2D tandem pump at revolving speeds varying from 500 r/min to 5000 r/min are shown and compared with the flow characteristics of the traditional pump with seven pistons in Table 1. The fluctuation of the flow curve depending on experimental data is obvious, but after the flow curve is filtered from clutter, it is close to zero. Although the curve still contains some influence from the ripples of revolving speed, it shows that the structural flow ripple is eliminated in the 2D pump. As Table 1 shows, about 4% of the flow ripple is coming from the structural ripple of the traditional seven-piston pump, and the rest is from reverse flow. The tendencies of the flow ripples after filtration and the simulated flow ripples in the tandem pump are opposite and are mainly caused by other factors. The experimental flow ripple is mainly determined by the ripple from the motor, and the motor runs more steadily as its speed increases, while the revolving speed in the simulated model is completely stable. The simulated flow ripple is mainly decided by reverse flow, and cannot be detected on the test bench of the experimental prototype.

5 Conclusions

A novel pump design which is highly integrated and force-balanced without structural flow pulsation was proposed and the principle was illustrated. The device has been designed so it has the potential to avoid the inevitable restrictions of the conventional axial piston pump, such as the sliding friction pairs, unbalanced forces, and structural flow ripple.

The spatial cam-follower mechanism as a vital part of the novel pump was prototyped and analyzed. Because one of the premises for realizing those advantages is a perfect motion transfer mechanism, a universal mathematical model of the contacting surface in the roller-cam rail mechanisms was constructed and calculated in the Matlab program. Then the precision of the cam was contrasted with the sample manufactured in the Geomagic program and verified through the motion test of the piston.

Then the no-load flow characteristics of the tandem pump were tested by analyzing the frequency spectrogram of the curves of flow and revolving speed. The clutter in the curve is considered mainly to originate from the fluctuation of the revolving speed. The curves were smoothed by applying a band-pass filter to remove the clutter for both to prove that the structural flow ripple of the tandem pump is close to zero.

As the sampling frequency of test bench is only 100 Hz, the details of the curve cannot be presented. Thus, through the Amesim program, the flow of the traditional pump with seven pistons and the 2D tandem pump are calculated and contrasted. In the comparison, the flow ripples in the experimental and simulation results for the tandem pump are smaller than those in simulation results for the traditional piston pump at low pressure.

Both the theoretical analysis and experimental results indicate that the surface of the cam rail is precise and the 2D pump has the potential advantage of eliminating sliding friction pairs and structural flow ripple.

Table 1 Contrast between simulation and experimental results

Revolving speed (r/min)	Experimental speed ripple (%)	Experimental flow ripple (%)	Speed ripple after filtration (%)	Flow ripple after filtration (%)	Simulated flow ripple of 2D pump (%)	Simulated flow ripple of traditional pump (%)
500	32.14	21.74	8.71	6.07	1.00	4.10
1000	20.56	14.60	11.42	4.10	1.00	4.50
2000	14.30	10.11	7.32	3.70	1.24	4.83
2500	11.02	8.29	6.60	4.60	1.38	5.09
3000	10.25	6.62	3.34	2.95	1.48	5.40
3500	10.81	7.89	5.55	3.24	1.70	5.64
4000	6.09	4.76	2.83	2.20	1.94	5.67
5000	4.90	2.77	1.68	0.85	2.60	6.60

References

Cho IS, 2015. A study on the optimum design for the valve plate of a swash plate-type oil hydraulic piston pump. *Journal of Mechanical Science and Technology*, 29(6): 2409-2413. https://doi.org/10.1007/s12206-015-0533-z

Du RL, Chen YL, Zhou H, et al., 2016. New distributing mechanism for high speed single-piston axial piston pump. *Journal of Zhejiang University (Engineering Science)*, 50(10):1902-1910 (in Chinese). https://doi.org/10.3785/j.issn.1008-973X.2016.10.009

Hong YS, Doh YH, 2004. Analysis on the friction losses of a bent-axis type hydraulic piston pump. *KSME International Journal*, 18(9):1668-1679. https://doi.org/10.1007/BF02990382

Ivantysynova M, 2008. Innovations in pump design–what are future directions? Proceedings of the 7th JFPS International Symposium on Fluid Power, p.59-64. https://doi.org/10.5739/isfp.2008.59

Luo XH, Niu ZH, Shi ZC, et al., 2011. Analysis and design of an axial piston water-pump with piston valve. *Journal of Mechanical Science and Technology*, 25(2):371-378. https://doi.org/10.1007/s12206-010-1214-6

Ma JE, Fang YT, Xu B, et al., 2010. Optimization of cross angle based on the pumping dynamics model. *Journal of Zhejiang University-SCIENCE A (Applied Physics & Engineering)*, 11(3):181-190. https://doi.org/10.1631/jzus.A0900417

Manring ND, Zhang YH, 2000. The improved volumetric-efficiency of an axial-piston pump utilizing a trapped-volume design. *Journal of Dynamic Systems, Measurement, and Control*, 123(3):479-487. https://doi.org/10.1115/1.1389311

Manring ND, Mehta VS, Raab FJ, et al., 2007. The shaft torque of a tandem axial-piston pump. *Journal of Dynamic Systems, Measurement, and Control*, 129(3):367-371. https://doi.org/10.1115/1.2719785

Manring ND, Mehta VS, Nelson BE, et al., 2013. Increasing the power density for axial-piston swash-plate type hydrostatic machines. *Journal of Mechanical Design*, 135(7):071002. https://doi.org/10.1115/1.4023924

Manring ND, Mehta VS, Nelson BE, et al., 2014. Scaling the speed limitations for axial-piston swash-plate type hydrostatic machines. *Journal of Dynamic Systems, Measurement, and Control*, 136(3):031004. https://doi.org/10.1115/1.4026129

Mehta VS, 2006. Torque Ripple Attenuation for an Axial Piston Swash Plate Type Hydrostatic Pump: Noise Consideration. PhD Thesis, University of Missouri-Columbia, Columbia, USA.

Navarro T, 2011. Volumetric Pump with Reciprocated and Rotated Piston. US Patent 7887308.

Ruan J, Burton RT, 2009. An electrohydraulic vibration exciter using a two-dimensional valve. *Proceedings of the Institution of Mechanical Engineers, Part I: Journal of Systems and Control Engineering*, 223(2):135-147. https://doi.org/10.1243/09596518JSCE634

Ruan J, Burton R, Ukrainetz P, et al., 2001. Two-dimensional pressure control valve. *Proceedings of the Institution of Mechanical Engineers, Part C: Journal of Mechanical Engineering Science*, 215(9):1031-1038. https://doi.org/10.1177/095440620121500903

Ruan J, Burton R, Ukrainetz P, 2002. An investigation into the characteristics of a two dimensional "2D" flow control valve. *Journal of Dynamic Systems, Measurement, and Control*, 124(1):214-220. https://doi.org/10.1115/1.1433480

Turner AJ, Ramsay K, Clark RE, et al., 2006. Development of high force electromechanical linear actuator for shift-by-wire automated manual transmissions. SAE 2006 World Congress & Exhibition. https://doi.org/10.4271/2006-01-0360

Vael GEM, van den Brink TL, Paardenkooper T, et al., 2003. Some design aspects of the floating cup hydraulic transformer. Proceedings of the Bath Workshop on Power Transmission and Motion Control, p.35-50.

Xu B, Ye SG, Zhang JH, et al., 2016. Flow ripple reduction of an axial piston pump by a combination of cross-angle and pressure relief grooves: analysis and optimization. *Journal of Mechanical Science and Technology*, 30(6):2531-2545. https://doi.org/10.1007/s12206-016-0515-9

Zhang JH, Wang D, Xu B, et al., 2018. Experimental and numerical investigation of flow forces in a seat valve using a damping sleeve with orifices. *Journal of Zhejiang University-SCIENCE A (Applied Physics & Engineering)*, 19(6):417-430. https://doi.org/10.1631/jzus.A1700164

中文概要

题　目：二维活塞泵用滚子-凸轮轨道机构的建模和验证

目　的：由于液压行业对高速重载的要求越来越高，传统轴向柱塞泵中存在的润滑与泄漏的矛盾也越发明显。针对传统轴向柱塞泵中因结构产生的倾斜力、低功率密度、恶劣的摩擦副工况、较大的流量脉动等限制，本文旨在提出一种具有内力平衡、功率密度高、无纯粹的滑动摩擦副且工况优秀、能消除结构性流量脉动等优点的二维活塞泵，并通过对其工作原理的详细分析，探讨其具有上述优点的理论依据。

创新点：1. 提出二维活塞泵；该泵利用二维运动转换机构中活塞部件的二维运动，同时实现了吸排油功能和配流功能，提高了集成化；通过其活塞旋转 1 周可以使泵吸排油 4 次的结构设计，提高了功率

密度；轴向与轴向对称的独特结构布局，实现了内力平衡，消除了传统轴向柱塞泵中无法消除的倾覆力偶；相对于传统轴向柱塞泵，吸排油与配流功能的集成减少了摩擦副的数量，且消除了纯粹的滑动摩擦副，打破了 PV 值的限制，意味着二维活塞泵有着实现更大流量压力分布的潜力。2. 提出二维活塞泵运动转换机构中的锥滚子-凸轮接触结构，优化二维活塞泵运动转换机构的受力条件；3. 建立二维活塞泵运动转换机构中锥滚子-凸轮接触副的通用型数学模型，通过运动学分析建立精确的凸轮表面模型（即二维活塞泵的运动学模型），为二维锥滚轮活塞泵的结构设计和进一步的静、动力学的研究提供理论基础。4. 消除结构性流量脉动。

方　法： 1. 通过对二维活塞泵结构与工作原理的理论分析，讨论其相对于传统轴向柱塞泵所具有的优点。2. 通过跑合实验，验证锥滚子-凸轮接触结构具有的受力条件。3. 通过运动学分析与空间几何关系变换推导，得到运动转换机构中具有普遍指导意义的接触副的通用数学模型。4. 通过实验曲线与理论曲线的对比，验证接触副数学模型的正确性与二维活塞泵所具有的消除结构流量脉动的潜力。5. 通过滤波处理与模拟仿真，验证二维活塞泵能否消除结构性流量脉动。

结　论： 1. 二维活塞泵具有功能集成化高、内力平衡、功率密度高、无纯粹的滑动摩擦副且能消除流量脉动的优点。2. 运动转换机构中锥滚子-凸轮接触结构具有更好的受力条件。3. 建立的接触副数学模型可以指导二维活塞泵中运动转换机构的加工，且对二维活塞泵进一步的运动学与动力学的研究具有指导意义。4. 二维活塞泵能消除结构性流量脉动。

关键词： 二维活塞泵；功能集成化；滚子-凸轮机构；数学模型；无结构性流量脉动。